Available online at www.sciencedirect.com

ScienceDirect

IFAC PapersOnline CONFERENCE PAPER ARCHIVE

IFAC PapersOnLine 54-16 (2021) 281–287

Trajectory Tracking SISO Marine Sampling Systems with Input and State Delays

Karl D. von Ellenrieder

Facoltà di Scienze e Tecnologie, Libera Università di Bolzano, 39100 BZ Italy (e-mail: kvonellenrieder@unibz.it).

Abstract: A globally asymptotically stable trajectory tracking controller for the control of single input, single output nonlinear systems with input and state delays is proposed in the context of marine sampling systems. A memoryless state feedback controller is designed under the assumption that the dynamics of the system can be upper bounded by a linear growth rate condition. A simulation example of a buoyancy controlled ocean measurement system is provided.

Copyright © 2021 The Authors. This is an open access article under the CC BY-NC-ND license (https://creativecommons.org/licenses/by-nc-nd/4.0/)

Keywords: Tracking, Delay systems, Nonlinear marine system control

1. INTRODUCTION

Owing to the costs and difficulty of accessing and deploying automatic marine sampling systems in remote regions, such systems must necessarily employ low power, slow speed, processors, sometimes also taking advantage of power conserving strategies, such as putting some sensory or communications subsystems to sleep for short time periods between measurements. Further, ocean sampling systems are often configured as a network control system, in which components of the system, e.g. the sensors, actuators and controllers, communicate through a shared band-limited digital communication network. The use of such networked control systems provides a flexible systems architecture and can simplify implementation, however, bandwidth limitations can lead to sampling and communications delays (Hespanha et al., 2007; Ogren et al., 2004). Thus, for marine applications, ensuring the closed loop stability of automatic control systems, especially nonlinear systems, in the presence of state and input delays is of paramount importance.

Approaches to the control of systems with time delays includes the works of Mazenc and Bliman (2006), Krstic (2009) and Karafyllis et al. (2016), which focus on nonlinear systems with input delays. The control of nonlinear systems with state delays is addressed by Jankovic (2010), Lin and Zhang (2019), Pongvuthithum et al. (2017), Pepe and Fridman (2017), Zhang et al. (2016) and Zhang et al. (2017). Lastly, the more general problem of controlling systems with time delays in both the input and state is studies by Bekiaris-Liberis and Krstic (2010), Pepe (2014), Zhou et al. (2012), Zhao and Lin (2020) and Marquez-Martinez and Moog (2004).

In general, there are two main approaches for the feedback control of nonlinear systems with input delays, the predictor approach, e.g. Karafyllis and Krstic (2013), and the emulation approach, in which one first disregards input delays and designs a controller to asymptotically stabilize the system and then studies the effects of the input delays on the closed loop system. Here, the stabilization approach proposed by Lin and Zhao (2020), which uses memoryless state feedback, is extended to solve a trajectory tracking control problem.

The organization of the paper is as follows. The mathematical principles behind the approach are presented in Section 2, the trajectory tracking controller is proposed in Section 3, a representative simulation is presented in Section 4 and some concluding remarks and possible future work are discussed in Section 5.

2. MATHEMATICAL PRELIMINARIES

Consider a single-input, single-output time-delay system of the form

$$\begin{aligned} \dot{x}_i(t) &= x_{i+1}(t-\delta_{i+1}) + \bar{f}_i(\boldsymbol{x}(t), \boldsymbol{x}(t-d), u(t-\delta_1)), \\ &\qquad i = 1, \ldots, n-1, \\ \dot{x}_n(t) &= u(t-\delta_1) + \bar{f}_n(\boldsymbol{x}(t), \boldsymbol{x}(t-d), u(t-\delta_1)), \\ y(t) &= x_1(t), \end{aligned} \tag{1}$$

where $\boldsymbol{x} = [x_1 \;\; x_2 \;\; \cdots \;\; x_n]^T \in \mathbb{R}^n$, $u \in \mathbb{R}$ and $y \in \mathbb{R}$ are the system state, input and output, respectively. The state with time delays is represented by the vector

$$\boldsymbol{x}(t-d) = [x_1(t-d_1) \;\; x_2(t-d_2) \;\; \cdots \;\; x_n(t-d_n)]^T, \tag{2}$$

where the real constants $d_i > 0$ and $\delta_i > 0$ represent state and integrator chain time delays, respectively. For $i = 1, \ldots, n$, the initial state is continuous over the time delay intervals $x_i(\theta) \in C([-\max\{\delta_i, d_i\}, 0], \mathbb{R})$, the f_i are smooth functions, and satisfy the following linear growth rate condition.

Assumption 1. For $i = 1, \ldots, n$, there exists a real constant $c \geq 0$ such that

$$|\bar{f}_i| \leq c \sum_{j=1}^{i} \left(|x_j(t)| + |x_j(t-d_j)| \right). \tag{3}$$

Under this assumption, a *memoryless* stabilizing control input of the form

2405-8963 Copyright © 2021 The Authors. This is an open access article under the CC BY-NC-ND license.
Peer review under responsibility of International Federation of Automatic Control.
10.1016/j.ifacol.2021.10.105

$$u = -\boldsymbol{K}\boldsymbol{x}, \tag{4}$$

where $\boldsymbol{K} > 0$ is a constant row vector, can be designed by rescaling the states and input in (1) by a time-like parameter L and then separating the resulting scaled state equations into a nominal linear system without time delays, which is perturbed by a nonlinear system with state, integrator chain and input time delays. Using the Feedback Domination Method (Chunjiang Qian et al., 2003; Qian and Lin, 2002) L is selected so that nonlinear part of the system is dominated by the nominal linear system.

In more detail, the scaling

$$\eta_i = \frac{x_i}{L^{i-1}}, \quad i = 1, 2, \ldots, n \quad \text{and} \quad v = \frac{u}{L^n}, \tag{5}$$

where $L \geq 1$, is used to transform (1) into the system

$$\begin{aligned} \dot{\eta}_i(t) &= L\eta_{i+1}(t) + Lh_i(\cdot) + f_i(\cdot), \\ &\qquad i = 1, \ldots, n-1, \\ \dot{\eta}_n(t) &= Lv(t) + Lh_n(v(t), v(t-\delta_1)) + f_n(\cdot), \\ y(t) &= \eta_1(t), \end{aligned} \tag{6}$$

with

$$\begin{aligned} h_i(\cdot) &:= \eta_{i+1}(t-\delta_{i+1}) - \eta_{i+1}(t), \\ &\qquad i = 1, \ldots, n-1, \end{aligned} \tag{7}$$

$$\begin{aligned} h_n(\cdot) &:= v(t-\delta_1) - v(t), \\ f_i(\cdot) &:= f_i(\boldsymbol{\eta}, \boldsymbol{\eta}(t-d), v(t-\delta_1)), \\ &= \frac{\bar{f}_i(\boldsymbol{x}, \boldsymbol{x}(t-d), u(t-\delta_1))}{L^{i-1}}, \end{aligned} \tag{8}$$

and $\boldsymbol{\eta}(t-d) = [\eta_1(t-d_1) \cdots \eta_n(t-d_n)]^T$.

The nominal linear system is obtained by taking $h_i(\cdot) = 0$ and $f_i(\cdot) = 0$, $\forall i$ in (6). The Backstepping Method can be used to design a linear feedback controller renders the closed loop nominal linear system globally asymptotically stable (GAS). This control input is given by

$$\begin{aligned} v(t) &= -\beta_n \xi_n(t), \\ &= -\bar{\beta}_1 \eta_1(t) - \cdots - \bar{\beta}_n \eta_n(t), \end{aligned} \tag{9}$$

where the gains are $\bar{\beta}_i := \beta_1 \cdots \beta_i > 0$, for $1 = 1, \ldots, n$,

$$\xi_i := \eta_i - \eta_i^*, \quad \eta_{i+1}^* := -\beta_i \xi_i, \quad i = 1, 2, \ldots, n, \tag{10}$$

and $\eta_1^* = 0$.

As (9) leaves the time derivative of the Lyapunov function

$$V_n(\eta) = \frac{1}{2}\left(\xi_1^2 + \cdots + \xi_n^2\right), \tag{11}$$

negative definite, i.e.

$$\dot{V}_n(\eta) \leq -2L\left(\xi_1^2 + \cdots + \xi_n^2\right), \quad \forall \xi_i \neq 0, \tag{12}$$

the closed loop nominal system is GAS.

Applying the control input (9) and the stabilizing function (11) to the scaled nonlinear system with time delays (6) gives

$$\dot{V}_n(\eta) \leq -2L\sum_{i=1}^{n} \xi_i^2 + L\sum_{i=1}^{n} \frac{\partial V_n}{\partial \eta_i} h_i(\cdot) + \sum_{i=1}^{n} \frac{\partial V_n}{\partial \eta_i} f_i(\cdot). \tag{13}$$

Define the maximum state and integrator chain/input delays as

$$\bar{d} := \max_{1 \leq i \leq n} \{d_i\} \quad \text{and} \quad \bar{\delta} := \max_{1 \leq i \leq n} \{\delta_i\}, \tag{14}$$

respectively. For times $t \geq \bar{\delta} + \bar{d}$, the last two terms in (13) are upper-bounded as shown below in (15)–(16), where $\xi_0 = 0$, $a_{i1}, \bar{a}_{i1}, b_{i1}, \bar{b}_{i1}$, $i = 1, \ldots, n$ are positive constants, which are independent of L, and $\tilde{a}_{if}, \tilde{b}_{i1}$, $i = 1, \ldots, n$ are positive constants independent of both L and $\bar{\delta}$ (Lin and Zhao, 2020).

The coefficients of the terms in (15)–(16) can be used to determine two important conditions that must be satisfied in order for the full nonlinear system with time delays to be stable:

1) the lower bounds of the time scaling parameter is

$$L \geq \frac{3}{2} \max_{1 \leq i \leq n} \left\{\tilde{a}_{if} + \tilde{b}_{if} + \tilde{b}_{i+1,f} + 1\right\}, \tag{17}$$

where $b_{n+1,1} = \tilde{b}_{n+1,f} = 0$, and

2) the maximum allowable input delay is $\bar{\delta} \leq \Delta_x$, where

$$\Delta_x := \min\left\{\frac{2}{3L(\bar{a}_{i1} + 2\bar{b}_{i1})}, \frac{2}{3(a_{i1} + 2b_{i1} + b_{i+1,1})}\right\}. \tag{18}$$

Provided that these two conditions hold, the following theorem establishes the GAS of the closed loop nonlinear system with time delays.

Theorem 1. (Lin and Zhao, 2020) Under Assumption 1 there exist positive constants $\bar{\beta}_1, \ldots, \bar{\beta}_n$, a gain $L \geq 1$ given by (17) and a constant $\Delta_x \geq 0$ given in (18), such that for $\delta_i \in [0, \Delta_x]$, where $i = 1, \ldots, n$, the memoryless state feedback controller

$$u(t) = -L^n \bar{\beta}_1 x_1(t) - L^{n-1} \bar{\beta}_2 x_2(t) \cdots - L\bar{\beta}_n x_n(t) \tag{19}$$

renders the time-delay nonlinear system (1) globally asymptotically stable (GAS).

The GAS of (1) is possible when the integrator chain time delays δ_i $(i = 2, \ldots, n)$ are small and the input time delay δ_1 is small. The state delays d_i may be large, but must be bounded.

Remark 1. Under Assumption 1, the closed loop system (1) with memoryless feedback (4) is forward-complete (Lin and Zhao, 2020).

3. TRACKING CONTROLLER DESIGN

Let $x_{1d}(t) \in C^n$ be a continuously differentiable desired trajectory (at least to order n) and define the tracking errors as

$$\tilde{x}_i(t) := x_i(t) - x_{1d}^{(i-1)}(t), \quad i = 1, \ldots, n, \tag{20}$$

where the superscript $(i-1)$ indicates the $(i-1)^{\text{th}}$ derivative, and the output error to be

$$\tilde{y} := x_1(t) - x_{1d}(t). \tag{21}$$

Theorem 2. Take $\bar{f}_i(\cdot) = 0$ for $i = 1, \ldots, n-1$ in (1). If the conditions given by (17) and (18) are satisfied, the corresponding closed loop tracking error system is rendered GAS by a controller of the form

$$u = \tau + x_{1d}^{(n)}(t) - \hat{f}_n(\boldsymbol{x}_d(t)), \tag{22}$$

where

$$\tau(t) = -L^n \bar{\beta}_1 \tilde{x}_1(t) - L^{n-1} \bar{\beta}_2 \tilde{x}_2(t) \cdots - L\bar{\beta}_n \tilde{x}_n(t), \tag{23}$$

$$\sum_{i=1}^{n} \frac{\partial V_n}{\partial \eta_i} h_i(\cdot) \leq \sum_{i=1}^{n} \left\{ \bar{\delta} \left(L\bar{a}_{i1} + a_{i1} \right) \xi_i^2 + L \int_{t-2\bar{\delta}}^{t} \bar{b}_{i1} \xi_i^2(s) \mathrm{d}s + \int_{t-\bar{\delta}}^{t} b_{i1} \left[\xi_i^2(s) + \xi_i^2(s-d_i) + \xi_{i-1}^2(s-d_i) \right] \mathrm{d}s \right\} \tag{15}$$

$$\sum_{i=1}^{n} \frac{\partial V_n}{\partial \eta_i} f_i(\cdot) \leq \sum_{i=1}^{n} \left\{ \tilde{a}_{if} \xi_i^2 + \tilde{b}_{if} \left[\xi_i^2(t-d_i) + \xi_{i-1}^2(t-d_i) \right] \right\} \tag{16}$$

$L \geq 1$, $\bar{\beta}_i > 0$ for $i = 1, \ldots, n$, and $\hat{f}_n(\boldsymbol{x}_d(t))$ is a model of $\bar{f}_n(\cdot)$ with desired state as input argument that satisfies Assumption 1.

Proof. Using (22) in (1), and taking $\bar{f}_i(\cdot) = 0$ for $i = 1, \ldots, n-1$, the time derivatives of the tracking errors can be written as

$$\begin{aligned} \dot{\tilde{x}}_i(t) &= \tilde{x}_{i+1}(t - \delta_{i+1}), \quad i = 1, \ldots, n-1, \\ \dot{\tilde{x}}_n(t) &= \tau(t - \delta_1) + \tilde{f}_n(\tilde{\boldsymbol{x}}(t), \tilde{\boldsymbol{x}}(t-d), \tau(t-\delta_1)), \\ \tilde{y}(t) &= \tilde{x}_1(t), \end{aligned} \tag{24}$$

where $\tilde{f}_n(\cdot)$ satisfies Assumption 1 in terms of the state errors, i.e.

$$|\tilde{f}_n| \leq c_n \sum_{j=1}^{n} \left(|\tilde{x}_j(t)| + |\tilde{x}_j(t-d_j)| \right), \tag{25}$$

for a real constant $c_n \geq 0$. Since the closed loop tracking error system (24) has the same form as (1), $\tilde{f}_n(\tilde{\boldsymbol{x}})$ satisfies Assumption 1, and τ has the form of a memoryless state error feedback controller, according to Theorem 1 the tracking controller (22) renders the closed loop system GAS.

□

4. ILLUSTRATIVE SIMULATIONS

4.1 The Cyclesonde Profiling System

Consider the control of a buoyancy-driven automatic profiler, which is used to collect data by vertically traversing the water column in the open ocean. An example of such a profiler is the cyclesonde (Fig. 1), which has been extensively used to perform measurements of coastal upwelling, bottom boundary layers, oceanic mixed layers, inertial waves and tides, see for example, Johnson et al. (1976); Mercado and Van Leer (1976); Price et al. (1978); Van Leer and Leaman (1978); Van Leer (1985). Multiple cyclesonde systems (typically four or five) are deployed to form a synoptic array over a volume of water. The systems can operate in water depths of up to 300 m for durations of weeks to months, depending on the water depth profiled and the frequency of profiling. Profiles are made on a preprogrammed schedule, with a cycle typically starting every one to four hours.

Several versions of the cyclesonde system were developed between the early 1970s and the mid 1980s. The main features of the system are:

1) a subsurface profiling *fish* (called the cyclesonde), which has a diameter of about 30 cm and a length of 2.5 m;
2) profiler-mounted sensors for measuring current velocity, conductivity, temperature and pressure;

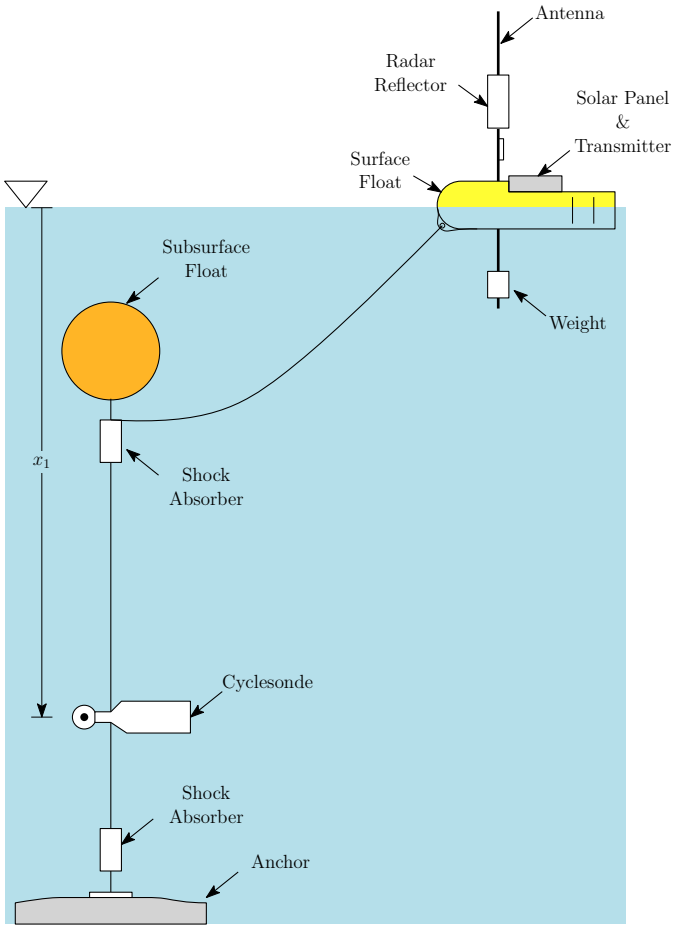

Fig. 1. The *cyclesonde*, an example of a buoyancy-controlled automatic profiler (Johnson et al., 1976).

3) a subsurface float and taut mooring line that constrains the motion of the system along the vertical direction; and
4) a surface float, which is used to telemeter the collected data to shore.

A steel cable is used for the lines from the surface float to the anchor, which permits an inductive modem to be used for communication between the cyclesonde and surface float. It is noted that more recently developed cable-crawler profiling systems (e.g. the McLane Moored Profiler), which are similar to the cyclesonde, exploit an inductive modem to also recharge the batteries of the subsurface profiler using power collected with the surface float solar panels (Alford et al., 2015). The vertical ascent/descent of the cyclesonde is controlled by using a pair of solenoids to inflate/deflate a helically coiled bladder with compressed helium, which is supplied with a specially modified SCUBA tank.

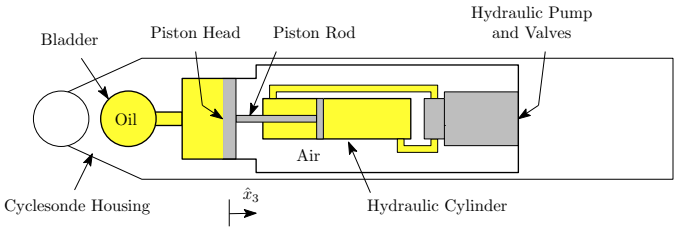

Fig. 2. Schematic of proposed buoyancy control system. The displacement of the piston from its position when the system is neutrally buoyant is $\hat{x}_3$.

Given the technology available at the time of its development, the design of the cyclesonde was very advanced. Recent progress in the fabrication of low power instrumentation, electrical motors, motor drivers, sensing and computing may make it possible to design a simpler version of the cyclesonde, which can lower its cost and improve its reliability.

Here, we explore the depth control of a cyclesonde via the use of a hydraulic-cylinder-driven piston that changes the volume of an elastic, oil-filled bladder to regulate the system's buoyancy (Fig. 2). Whereas the original design of the cyclesonde can only be operated for as long as its limited helium supply lasts, this approach could permit the cyclesonde to be run indefinitely, provided its surface float can be configured to electrically recharge the underwater portion of the system using an inductive modem, as discussed above.

4.2 The piston model

Here we use the reduced model for the motion of a hydraulic piston proposed by Ruderman (2017),

$$\dot{\hat{x}}_3 = \frac{P_L \bar{A} - f_s(\dot{\hat{x}}_3) + F_L}{m_p}, \tag{26}$$

where $\hat{x}_3$ is the displacement of the piston from its position when the system is neutrally buoyant (positive when the volume of the bladder decreases), m_p is the mass of the piston-rod assembly, F_L is the external load acting on the face of the piston head (see Fig. 2), $P_L\bar{A}$ is the force generated by the hydraulic cylinder and the function $f_s(\dot{\hat{x}}_3)$ represents the forces of Coulomb and linear viscous friction acting on the small piston inside the hydraulic cylinder.

The external force acting on the face of the piston head is caused by the pressure of the surrounding water and the forces of Coulomb and linear viscous friction acting on the larger piston head. The hydraulic-cylinder-driven piston and bladder are a sealed, closed system with air on one side of the piston head and oil on the other. It is assumed that when $\hat{x}_3 = 0$ the air inside the piston cylinder is at atmospheric pressure. When $\hat{x}_3 > 0$, the air is compressed increasing its pressure and when $\hat{x}_3 < 0$, the air expands so that its pressure decreases. This air pressure effect opposes the motion of the piston, but at large depths will be a small fraction of the total force acting on the piston head. The external load acting on the piston head is modeled as

$$F_L = A\left[\rho g x_1 - \frac{p_{\text{atm}} A \hat{x}_3}{(V_0 - A\hat{x}_3)}\right] - f_s(\dot{\hat{x}}_3), \tag{27}$$

where A is the area of face of the the piston head, ρ is the density of seawater, g is gravitational acceleration, x_1 is the profiler depth (positive in the downward direction), V_0 is the volume of the air in the buoyancy control mechanism when $\hat{x}_3 = 0$ and the forces of Coulomb and linear viscous friction acting on the larger piston head are assumed to be about the same as those acting on the small piston inside the hydraulic cylinder.

The Stribeck model (28) is commonly used to estimate the Coulomb and linear viscous friction forces acting on the piston, where $F_c > 0$ is the Coulomb friction coefficient, $F_s > F_c$ is the *stiction* coefficient, $\sigma > 0$ is the linear friction coefficient, and $\gamma \neq 0$ and $\chi > 0$ are Stribeck shape factors (Márton et al., 2011; Owen and Croft, 2003; Ruderman, 2017). See Table 1 for typical values of these coefficients associated with hydraulic cylinders commonly used in robotics applications.

Table 1. Typical values of the parameters in (28), after Ruderman (2017).

Parameter	Value [units]
F_c	600 N
F_s	900 N
σ	2000 kg/s
γ	0.8
χ	0.02 m/s

Lastly, take the control input be $\hat{u} = P_L\bar{A}/m_p$ and define

$$\hat{f}_3(\boldsymbol{x}) := \frac{-2f_s(\dot{\hat{x}}_3) + F_L}{m_p} \tag{29}$$

4.3 Cyclesonde equations of motion

The equations of motion can be written as

$$\begin{aligned} \dot{x}_1 &= x_2, \\ \dot{x}_2 &= \frac{(\rho - \rho_{\text{oil}})Ag}{m}\hat{x}_3, \\ \dot{\hat{x}}_3 &= \hat{u} + \hat{f}_3(\boldsymbol{x}), \\ y &= x_1, \end{aligned} \tag{30}$$

where m is the mass of the profiler, ρ_{oil} is the density of the oil and x_2 is its ascent/descent rate. The system output is the depth of the profiler $y = x_1$. Profiling buoys are typically operated at low speed. A typical profiling speed of the cyclesonde is about 10 cm/sec (Van Leer and Leaman, 1978). Owing to the low profiling speed and acceleration, both the drag and the added mass of the cyclesonde are neglected in the equations of motion.

Let $a_0 = (\rho - \rho_{\text{oil}})Ag/m$ and define

$$x_3 := a_0\hat{x}_3, \quad u := a_0\hat{u}, \quad \text{and} \quad f_3 := a_0\hat{f}_3,$$

so that (30) becomes

$$f_s(\dot{\hat{x}}_3) = \tanh\left(\dot{\hat{x}}_3\right)\left[F_c + (F_s - F_c)\exp\left(-|\dot{\hat{x}}_3|^{\gamma}\chi^{-\gamma}\right)\right] + \sigma\dot{\hat{x}}_3 \tag{28}$$

$$\begin{aligned} \dot{x}_1 &= x_2, \\ \dot{x}_2 &= x_3, \\ \dot{x}_3 &= u + f_3(\boldsymbol{x}). \end{aligned} \tag{31}$$

The density of seawater is about $\rho = 1025.9$ kg/m^3 and gravitational acceleration is $g = 9.81$ m/s^2. Let the diameter of the piston face be 20 cm and assume that mineral oil is used as the working fluid, so that $\rho_{\text{oil}} = 870$ kg/m^3. The total mass of the cyclesonde is anticipated to be about $m = 50$ kg. With these values it can be seen that $a_0 = 0.96$ m/s^2. Therefore, we will take $a_0 \approx 1.0$, so that $x_3 = \hat{x}_3$, $u = \hat{u}$, and $f_3 = \hat{f}_3$, which implies that (30) and (31) are equivalent.

The cyclesonde can be operated from within 15 m of the surface to within 1 m of the seafloor (Van Leer and Leaman, 1978). Here, we simulate the case of a cyclesonde operating in approximately 116 m of water. The profiler starts at an initial depth of $x_1(0) = 15$ m and is commanded to follow the desired profile

$$x_{1d}(t) = x_{10} - A_c \cos\left(\frac{2\pi}{T_c}t\right), \tag{32}$$

where $x_{10} = 65$ m and $A_c = 50$ m. The desired speed of the cyclesonde is determined by taking the time derivative of (32), which gives

$$\dot{x}_{1d}(t) = \frac{2\pi A_c}{T_c}\sin\left(\frac{2\pi}{T_c}t\right). \tag{33}$$

The period of a cycle T_c is determined by setting the root mean square value of $\dot{x}_{1d}(t)$ to 10 cm/s, i.e. by solving the relation

$$\frac{2\pi A_c}{\sqrt{2}T_c} = 10 \text{ cm/s}, \tag{34}$$

to get $T_c = 2.2214 \times 10^3$ s. The initial conditions of the remaining states are $x_2(0) = 0$ m/s and $x_3(0) = A_c(2\pi/T_c)^2$ m/s^2. Using simple hand-tuning for the system without time delays, the controller gains were selected as $\bar{\beta}_1 = 80$, $\bar{\beta}_2 = 10$, $\bar{\beta}_3 = 0.5$. The response of the system without time delays was found to be insensitive to the value of $\bar{\beta}_3$.

The sampling rate typically used during cyclesonde deployments is about 1 Hz (Van Leer and Leaman, 1978). Through manual tuning of the simulation parameters, the time delays were selected to be $\mathrm{d}_1 = 12.5$ ms, $\mathrm{d}_2 = 12.5$ ms, $\mathrm{d}_3 = 12.5$ ms and $\delta_1 = 20$ ms. The simulation was unstable for tested values larger than these. The selected delays are thus about two orders of magnitude smaller than the anticipated sample rate of 1 Hz.

The tracking errors and corresponding control input of the closed loop system are shown in Figs. 3–5. As can be seen in Fig. 3, the magnitudes of the control inputs for the cases examined is about the same. The magnitude of the control input is dominated by the force required to maintain the position of the piston as the hydrostatic pressure increases with increasing depth x_1.

As can be seen in Figs. 4–5, when there are no time delays and $L = 1$, the system tracks the desired trajectory with an error amplitude of about 2 mm. When the delays are included, and $L = 1$ (which corresponds to a system without compensation for time delay), the amplitude of the error is about 200 time larger, i.e. about 0.4 m. With $L = 2$ and $L = 3.5$ the amplitude of the error reduces to about the same as the system without time delay. The simulation cases examined for $L > 3.5$ were unstable.

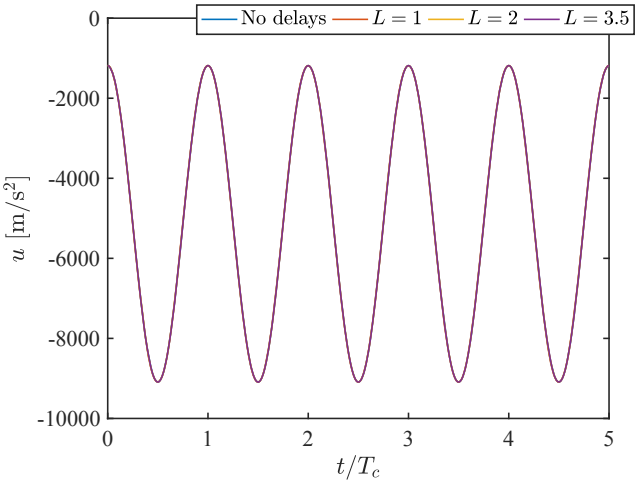

Fig. 3. Control input u of the buoyancy-driven profiler when tracking the sinusoidal trajectory (32) with no time delays, $L = 1$, $L = 2$ and $L = 3.5$.

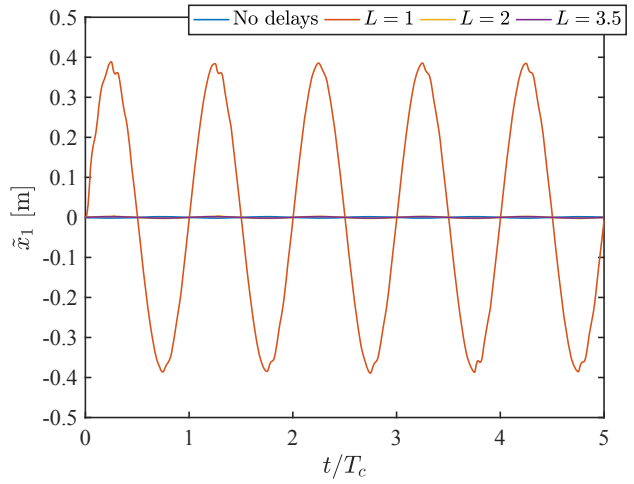

Fig. 4. Tracking error $\tilde{x}_1$ of the buoyancy-driven profiler when tracking the sinusoidal trajectory (32) with no time delays, $L = 1$, $L = 2$ and $L = 3.5$.

5. CONCLUDING REMARKS

The trajectory tracking control of a single-input, single-output system with input and state delays is addressed,

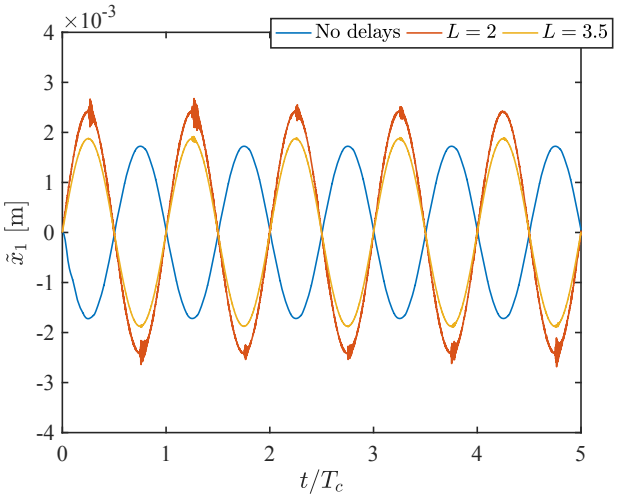

Fig. 5. Tracking error $\tilde{x}_1$ of the buoyancy-driven profiler when tracking the sinusoidal trajectory (32) with no time delays, $L = 2$ and $L = 3.5$.

with an eye towards applications for the control of marine sampling systems. Under the assumption that the system dynamics can be upper bounded using a linear growth rate condition, it is shown that the closed loop tracking error is globally asymptotically stabilizable using memoryless state feedback. The tracking control of a buoyancy controlled profiling system is provided as an illustrative example of the method. While the method appears to work well in reducing the tracking errors caused by time delays, the maximum time delays found in simulation were much shorter than the sampling rate of the system. Future work will explore how to analytically quantify the permissible time delays and time scaling parameter, as well as the extension of the approach to multiple input multiple output systems, and systems in strict feedback nonlinear system form.

REFERENCES

Alford, M.H., McGinnis, T., and Howe, B.M. (2015). An inductive charging and real-time communications system for profiling moorings. *Journal of Atmospheric and Oceanic Technology*, 32(12), 2243–2252.

Bekiaris-Liberis, N. and Krstic, M. (2010). Stabilization of linear strict-feedback systems with delayed integrators. *Automatica*, 46(11), 1902–1910.

Chunjiang Qian, Schrader, C.B., and Wei Lin (2003). Global regulation of a class of uncertain nonlinear systems using output feedback. In *Proc. American Control Conference*, volume 2, 1542–1547. doi: 10.1109/ACC.2003.1239810.

Hespanha, J.P., Naghshtabrizi, P., and Xu, Y. (2007). A survey of recent results in networked control systems. *Proceedings of the IEEE*, 95(1), 138–162.

Jankovic, M. (2010). Recursive predictor design for state and output feedback controllers for linear time delay systems. *Automatica*, 46(3), 510–517.

Johnson, W.R., Van Leer, J.C., and Mooers, C.N. (1976). A cyclesonde view of coastal upwelling. *Journal of Physical Oceanography*, 6(4), 556–574.

Karafyllis, I. and Krstic, M. (2013). Stabilization of nonlinear delay systems using approximate predictors and high-gain observers. *Automatica*, 49(12), 3623–3631.

Karafyllis, I., Malisoff, M., Mazenc, F., and Pepe, P. (2016). Stabilization of nonlinear delay systems: A tutorial on recent results. *Recent Results on Nonlinear Delay Control Systems*, 1–41.

Krstic, M. (2009). Input delay compensation for forward complete and strict-feedforward nonlinear systems. *IEEE Transactions on Automatic Control*, 55(2), 287–303.

Lin, W. and Zhang, X. (2019). A dynamic feedback framework for control of time-delay nonlinear systems with unstable zero dynamics. *IEEE Transactions on Automatic Control*, 65(8), 3317–3332.

Lin, W. and Zhao, C. (2020). Global stabilization by memoryless feedback for nonlinear systems with a small input delay and large state delays. *IEEE Transactions on Automatic Control*.

Marquez-Martinez, L. and Moog, C.H. (2004). Input-output feedback linearization of time-delay systems. *IEEE Transactions on Automatic Control*, 49(5), 781–785.

Márton, L., Fodor, S., and Sepehri, N. (2011). A practical method for friction identification in hydraulic actuators. *Mechatronics*, 21(1), 350–356.

Mazenc, F. and Bliman, P.A. (2006). Backstepping design for time-delay nonlinear systems. *IEEE Transactions on Automatic Control*, 51(1), 149–154.

Mercado, A. and Van Leer, J. (1976). Near bottom velocity and temperature profiles observed by cyclesonde. *Geophysical Research Letters*, 3(10), 633–636.

Ogren, P., Fiorelli, E., and Leonard, N.E. (2004). Cooperative control of mobile sensor networks: Adaptive gradient climbing in a distributed environment. *IEEE Transactions on Automatic control*, 49(8), 1292–1302.

Owen, W.S. and Croft, E.A. (2003). The reduction of stick-slip friction in hydraulic actuators. *IEEE/ASME transactions on mechatronics*, 8(3), 362–371.

Pepe, P. (2014). Direct and converse lyapunov theorems for functional difference systems. *Automatica*, 50(12), 3054–3066.

Pepe, P. and Fridman, E. (2017). On global exponential stability preservation under sampling for globally lipschitz time-delay systems. *Automatica*, 82, 295–300.

Pongvuthithum, R., Rattanamongkhonkun, K., and Lin, W. (2017). Asymptotic regulation of time-delay nonlinear systems with unknown control directions. *IEEE Transactions on Automatic Control*, 63(5), 1495–1502.

Price, J.F., Mooers, C.N., and Van Leer, J.C. (1978). Observation and simulation of storm-induced mixed-layer deepening. *Journal of Physical Oceanography*, 8(4), 582–599.

Qian, C. and Lin, W. (2002). Output feedback control of a class of nonlinear systems: a nonseparation principle paradigm. *IEEE Transactions on Automatic Control*, 47(10), 1710–1715.

Ruderman, M. (2017). Full-and reduced-order model of hydraulic cylinder for motion control. In *IECON 2017-43rd Annual Conference of the IEEE Industrial Electronics Society*, 7275–7280. IEEE.

Van Leer, J. and Leaman, K. (1978). Physical oceanographic research using the attended profiling current meter (apcm) and the cyclesonde. In *Proceedings of*

the 1978 IEEE First Working Conference on Current Measurement, volume 1, 77–93. IEEE.

Van Leer, J.C. (1985). Automatic arctic profiling system for oceanography under ice. In *Oceans Conference Record (IEEE)*, 433–436. Institute of Electrical and Electronics Engineers Inc.

Zhang, X., Lin, W., and Lin, Y. (2016). Nonsmooth feedback control of time-delay nonlinear systems: A dynamic gain based approach. *IEEE Transactions on Automatic Control*, 62(1), 438–444.

Zhang, X., Lin, W., and Lin, Y. (2017). Dynamic partial state feedback control of cascade systems with time-delay. *Automatica*, 77, 370–379.

Zhao, C. and Lin, W. (2020). Memoryless linear feedback control for a class of upper-triangular systems with large delays in the state and input. *Systems & Control Letters*, 139, 104679.

Zhou, B., Li, Z.Y., Zheng, W.X., and Duan, G.R. (2012). Stabilization of some linear systems with both state and input delays. *Systems & Control Letters*, 61(10), 989–998.